

# Spatial distribution of Spontaneous Parametric Down-Converted Photons for higher order Optical Vortices

Shashi Prabhakar,<sup>1</sup> Salla Gangi Reddy,<sup>1</sup> A Aadhi,<sup>1</sup> Ashok Kumar,<sup>2</sup> Chithrabhanu P,<sup>1</sup> G. K. Samanta<sup>1</sup> and R. P. Singh<sup>1</sup>  
<sup>1</sup>*Physical Research Laboratory, Navrangpura, Ahmedabad. 380009, India. and*  
<sup>2</sup>*Instituto de Física, Universidade de São Paulo, São Paulo, 66318, Brazil.*

(Dated: December 2, 2024)

We make a source of entangled photons (SEP) using spontaneous parametric down-conversion (SPDC) in a non-linear crystal and study the spatial distribution of photon pairs obtained through down-conversion of different modes of light including higher order vortices. We have observed that for the Gaussian pump, the thickness of the SPDC ring varies linearly with the radius of pump beam. While for the optical vortex beams, two concentric SPDC rings are formed, however, it happens above a critical radius of the vortex beam. The FWHM of SPDC rings increases with increase in the order of optical vortex beams. The presence of a critical beam width for the optical vortices as well as the observed full width at half maximum of the SPDC rings are supported by our numerical results also.

PACS numbers: 050.4865, 190.4975, 42.65.-k, 42.65.Yj

## I. INTRODUCTION

The process of spontaneous parametric down-conversion (SPDC) has been used extensively for the generation of entangled photon pairs in many recent experiments. The purpose of these experiments range from Bell's inequality violation [1] to the implementation of quantum information protocols [2]. In the process of SPDC, a laser pump beam photon interacts with second-order nonlinear  $\chi^{(2)}$  crystal, gets annihilated and gives rise to the emission of two photons. These two photons are generated simultaneously and follow the law of energy and momentum conservation. The phenomena of SPDC was first observed by Burnham and Weinberg [3] and theoretically studied by Hong Ou and Mandel [4].

The photon pairs generated through SPDC are entangled in the spatial degree of freedom i.e. position-momentum entanglement including entanglement in orbital angular momentum (OAM) [5]. This spatial entanglement can be described by a multi-dimensional Hilbert space [6–8], compared to the case of polarization entanglement which is limited to two dimensions [9]. These photon pairs have been found to be entangled in time-bin also [10].

Optical vortices (OV) carry a dark core in a bright background [11]. If there is a phase change of  $2\pi l$  around the point of darkness, it is called a vortex of topological charge  $l$ , where  $l$  is an integer. The sense of rotation determines the sign of topological charge of the vortex. A beam with such a phase structure has a helical wavefront and, therefore, carries an OAM of  $l\hbar$  per photon [12] for a vortex of topological charge  $l$ . These beams have found a variety of applications, such as in the optical trapping of atoms [13], optical tweezing and spanning [14], optical communication [5], imaging [15], and quantum information and computation [7].

For any application of entangled photons generated through the SPDC, it is important to know the spatial

distribution of photons arising from the SPDC process. There are reports available in which spatial distribution of photons when pumped with Gaussian beam have been discussed [16, 17], although a detailed study is missing even for Gaussian pump beam. However, for OV beams, spatial distribution of down-converted photons have not been studied so far. The theory regarding the spatial distribution of photons due to optical vortex pump has also not been studied, which is still a problem to be studied.

With the availability of low noise and high quantum-efficiency Electron-Multiplying CCDs (EMCCD), the experiments with low photon level imaging has become possible [18]. We have carried out experimental studies using EMCCD along with numerical studies to observe the shape of the SPDC ring formed by the Gaussian beam as well as optical vortex beams. The theory regarding the SPDC has been discussed in section II, experiments performed in section III and results in section IV and then finally we conclude in section V.

## II. THEORY

The intensity distribution of optical vortex can be written as

$$I_l(x, y) = I_0(x^2 + y^2)^{|l|} \exp\left(-\frac{x^2 + y^2}{\sigma^2}\right) \quad (1)$$

where  $\sigma$  is the beam radius,  $I_0$  is the maximum intensity in the bright ring and  $l$  is the topological charge of optical vortex. A look at Eq. 1 shows that the Gaussian beam is a special case of optical vortex with  $l = 0$ .

The nonlinear effects in crystals have been exploited in a number of applications such as frequency doubling, optical parametric oscillation and the SPDC [19]. When a nonlinear crystal, for example Beta-Barium Borate (BBO), with non-zero second order electric susceptibility ( $\chi^{(2)}$ ) is pumped by an intense laser, a *pump* photon

(frequency  $\omega_p$  and wave-vector  $\mathbf{k}_p$ ) splits into a photon pair called *signal* and *idler*. The energy and momentum conservation provide us with

$$\hbar\omega_p = \hbar\omega_s + \hbar\omega_i, \quad (2)$$

$$\mathbf{K}_p = \mathbf{K}_s + \mathbf{K}_i, \quad (3)$$

where  $\omega$  is the frequency,  $\mathbf{k}$  is the wave vector and suffices  $s$  and  $i$  denote signal and idler photons respectively. The phase matching is determined by the frequency of pump laser beam, and the orientation of crystal optic axis with respect to the pump. Eq. 2 can be simplified as

$$\frac{1}{\lambda_p} = \frac{1}{\lambda_s} + \frac{1}{\lambda_i}, \quad (4)$$

where  $\lambda_p$ ,  $\lambda_s$  and  $\lambda_i$  denote wavelengths of pump, signal and idler photons respectively. Equation 3 can be written as

$$\begin{aligned} k_p &= k_s \cos(\phi_s) + k_i \cos(\phi_i) \\ k_s \sin(\phi_s) &= k_i \sin(\phi_i) \end{aligned} \quad (5)$$

where  $\phi_s$  is the angle between  $\mathbf{K}_p$  and  $\mathbf{K}_s$  and  $\phi_i$  is the angle between  $\mathbf{K}_p$  and  $\mathbf{K}_i$ . Equation 5 includes crystal optic axis  $\Theta$  (angle between pump beam propagation and optic axis) and suitable refractive indices for pump, signal and idler photons.

In Fig. 1, we have given the sketch of the SPDC photon pair generation in non-collinear type-I SPDC process.  $\mathbf{C}$  denotes the crystal optic axis. The angular separation between  $\mathbf{K}_p$  and  $\mathbf{K}_s$  is due to energy and phase-matching conditions (Eq. 5) required for the SPDC process. We have also shown generation of a pair of signal and idler photons and forming a ring centered around  $\mathbf{K}_p$ . In the present case, we have assumed that the pump beam has same horizontal and vertical widths.

We plan to study the degenerate or near-degenerate case in which both the signal and idler have almost same

wavelength. In this case, due to degeneracy, we will obtain only one SPDC ring corresponding to the degenerate wavelength. For our study, we have used  $810 \pm 5$  nm IF.

Numerical simulation has been performed by solving the phase-matching Eqs. 4 and 5 to obtain the spatial distribution of generated photons. We have used a negative uniaxial BBO crystal with non-linear coefficient  $d_{\text{eff}} = 2.00$  pm/V for  $e \rightarrow o + o$  type ( $e$ : extraordinary,  $o$ : ordinary) interaction. Our experimental parameters are  $\lambda_p = 405$ nm,  $\lambda_{s,i} = 810 \pm 5$  nm (allowed by IF),  $\Theta = 29.7^\circ$ , and refractive indices of BBO crystal for appropriate wave-lengths. With these parameters, Eq. 5 has been solved to obtain  $\phi_s$  and  $\phi_i$  by using Runge-Kutta method. After obtaining  $\phi_s$  and  $\phi_i$ , we can draw the SPDC ring for signal and idler photons centered at the pump beam. The radius of SPDC ring depends on the distance between crystal and EMCCD. As the intensity of SPDC ring is proportional to the pump intensity, the contribution due to the whole pump beam is evaluated and integrated. The contribution due to wave-length allowed by the IF has been considered in our numerical simulation. However, we have not considered the asymmetry in the SPDC ring due to the crystal length.

### III. EXPERIMENTAL SETUP

The experimental set-up to study SPDC photon distribution generated by Gaussian as well as optical vortex pump beam is shown in Fig. 2. The astigmatism and elliptical divergence of diode laser (RGBLase 405 nm, 50 mW) have been removed by using a combination of lenses. The collimated beam is then sent to Hamamatsu LCOS SLM (X-10468-05), which is interfaced with computer (PC1). Blazed holograms have been used to generate OV having more power in first diffraction order [20]. We have selected the first diffracted order by using aperture A3. We have used polarizer (P) and half-wave plate (HWP) to select and rotate the polarization of pump beam respectively. BBO crystal ( $6 \times 6 \times 5$  mm<sup>3</sup>) with optics axis at  $29.7^\circ$  is used for this study. As the size of OV of higher order becomes bigger than the size of the crystal, we have used a lens L1 ( $f=15$  cm) to loosely focus the vortex beam on the crystal. The BBO crystal is mounted on a rotation stage, so that phase-matching angle can be achieved by rotating the crystal along its optic axis. After achieving phase-matching, the crystal remains unaltered for all observations.

When phase-matched, the output cone makes half angle of  $\sim 4^\circ$  with pump direction  $\mathbf{K}_p$ . The BBO crystal is kept in such a way that it can down-convert only vertically polarized light. This shows that when angle of the HWP is  $0^\circ$  ( $45^\circ$ ), then we will get (not get) down-converted photons. Image of the down-converted ring is recorded by Andor iXon3 EMCCD camera using an imaging lens of focal length 5 cm. We have used the EMCCD in background correction mode. In this mode, background is obtained when  $\lambda/2$  plate is at  $45^\circ$  and

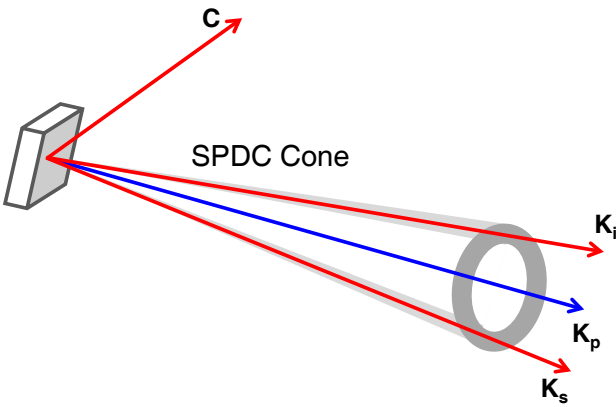


FIG. 1. (Color online) Sketch diagram for the SPDC ring emission obtained by pumping BBO crystal with pump beam.

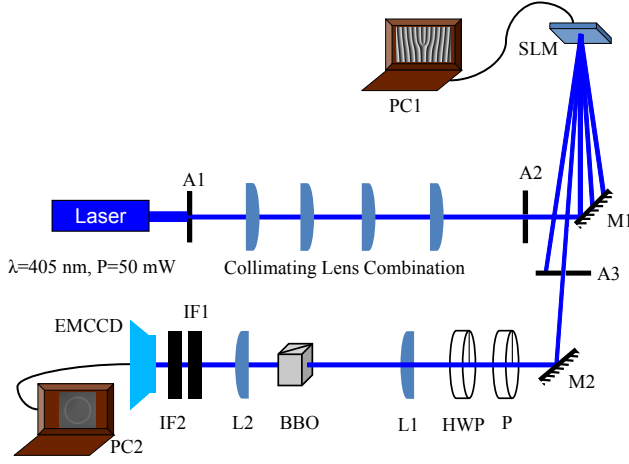


FIG. 2. (Color online) Experimental setup for the study of SPDC photon pair distribution with optical vortex as pump beam.

signal is obtained when  $\lambda/2$  plate is at  $0^\circ$ . The central bright spot in experimental observations show the unfiltered pump beam by the IF (IF1 and IF2). This could not be subtracted while subtracting the background due to shift in its position during the rotation of HWP from  $45^\circ$  to  $0^\circ$ . This filter passes only the down-converted photons of wave-length  $810 \pm 5$  nm and blocks the pump photons of wave-length 405 nm. Two IFs have been used to reduce the pump photons better.

The size of pump beam has been measured by imaging the beam at the position of crystal with Point-Grey (FL2-20S4C) CCD camera. The images obtained from CCD camera are read in Matlab for further processing. 2-D curve fitting is used to obtain the best-fit of the intensity distribution with Eq. 1 that provide us for beam-width of the pump ( $\sigma_{\text{pump}}$ ). For our numerical calculation, we have used the best-fit value of  $\sigma_{\text{pump}}$  obtained experimentally.

#### IV. RESULT AND DISCUSSION

The objective of the experimental work is to characterize the spatial distribution of degenerate SPDC photon pairs produced by higher order vortices and verify with the results obtained from numerical calculations. Before pumping the nonlinear crystal with high order vortices, we study the distribution of SPDC photons generated by the Gaussian beam of different widths.

To make a comparison of spatial distribution of down-converted photons due to the Gaussian and vortex beams, the Gaussian beam is generated using the SLM by transferring the blazed grating hologram of topological charge 0 to the SLM. To vary the width of the Gaussian beam, we have used the beam at different propagation distances from the SLM (150 cm to 350 cm in the steps

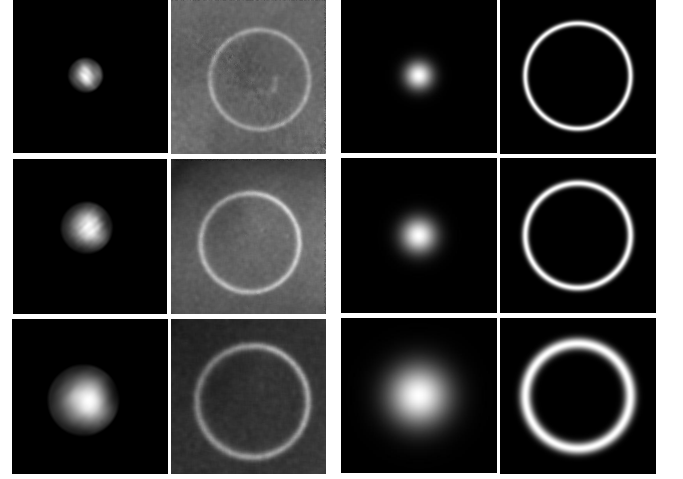


FIG. 3. SPDC ring due to a gaussian pump beam. Experimental (left) and Numerical (right). These images have been obtained at distances 150 cm, 250 cm and 350 cm from the SLM.

of 50 cms). As the size of beam was lower than the aperture of the crystal at 350 cm from the SLM, we have not used the lens (L1) in experimental setup. The experimentally and numerically obtained SPDC rings are shown in Fig. 3. We observe an increase in thickness of the SPDC ring as the pump beam size increases.

To obtain a quantitative variation of SPDC ring, we use the line profile through the SPDC rings along the center. Numerically, we have observed that the SPDC ring fits with a Gaussian function. To calculate the width of SPDC ring ( $\sigma_{\text{ring}}$ ), the profiles obtained are fitted with a Gaussian function as in Eq. 1 for  $l=0$ . The variation of thickness of the SPDC rings with the size of the pump beam is shown in Fig. 4. Numerical and experimental results are found to be in good agreement with each other.

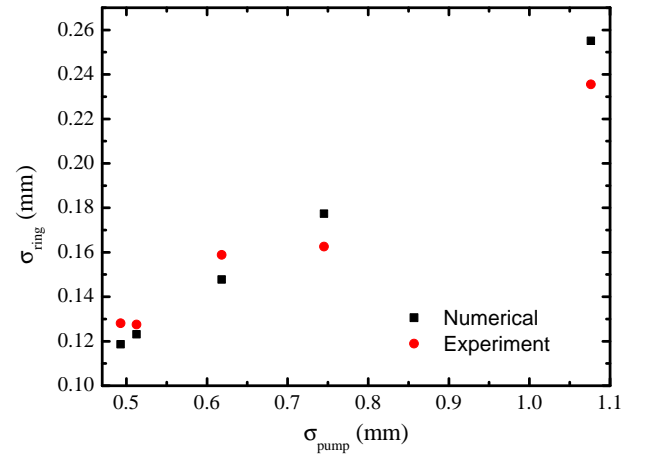


FIG. 4. (Color online) Variation of  $\sigma_{\text{ring}}$  with  $\sigma_{\text{pump}}$ . The curve shows linear variation.

We find our results are similar to the one obtained earlier [16].

Next, we take up OV as pump beam. As the size of optical vortex goes beyond the aperture of BBO crystal, we have used lens (L1) to loosely focus it. It has been observed that the SPDC ring due to optical vortex forms two concentric bright rings with non-zero intensity in middle. The SPDC rings due to optical vortices are shown in Fig. 5. From these images, we can observe the increase in thickness of the SPDC ring. The experimentally obtained SPDC rings from EMCCD camera have been verified with the numerical simulation.

With the increase in topological charge of vortices, the full width at half maximum (FWHM) of the ring in-

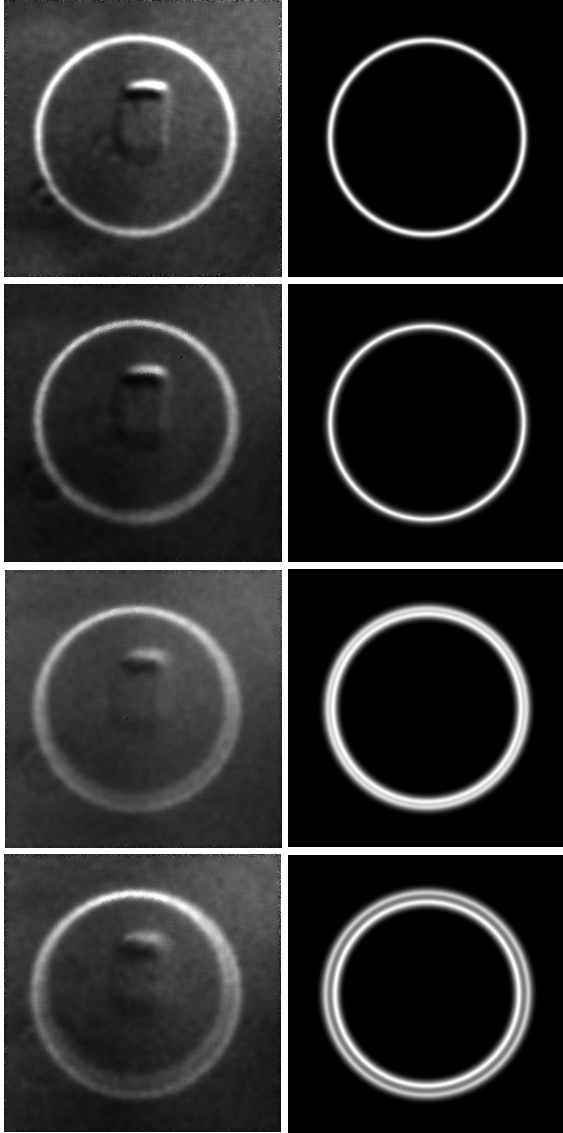


FIG. 5. Experimental (left) and Numerical (right) SPDC rings due to a optical vortex pump beam for order 1, 3, 6 and 9. Spot in the center of experimental images correspond to the unfiltered pump beam.

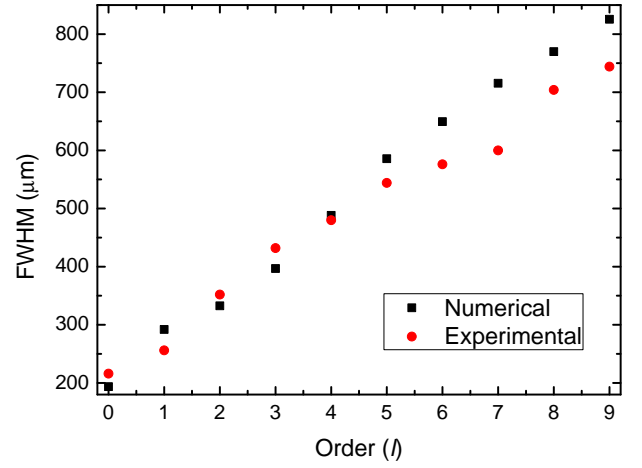


FIG. 6. (Color online) Variation for FWHM of SPDC ring for optical vortex pump beam.

creases. The separation between the inner and outer ring also increases with the increase in order as shown in Fig. 6. However, we can observe the asymmetry caused due to the crystal length. This is one of the factors which affects the selection of entangled photons and consequently the total coincidence counts.

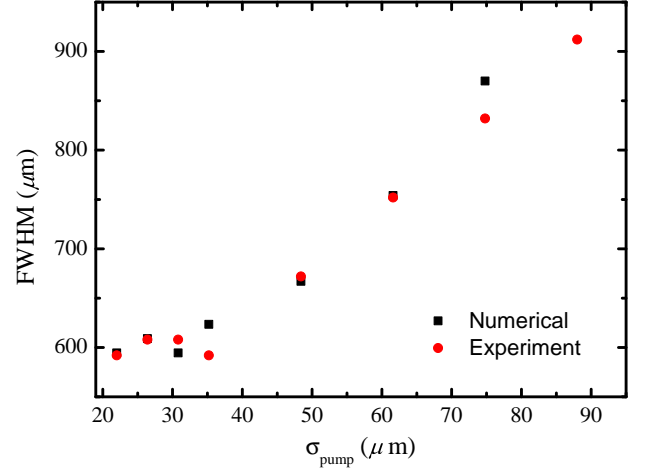


FIG. 7. (Color online) Variation for FWHM of SPDC ring for optical vortex pump beam of order  $l=2$ .

We have also observed that if  $\sigma_{\text{pump}}$  is lower than a particular value for the OV of topological charge  $l$ , then there will not be any change in FWHM. This variation has been studied by varying  $\sigma_{\text{pump}}$  and keeping the order  $l$  fixed. We have observed that FWHM of the ring starts increasing only when  $\sigma_{\text{pump}}$  is more than the critical beam size. The variation of FWHM of SPDC ring for order  $l=2$  with  $\sigma_{\text{pump}}$  is shown in Fig. 7. In case of OV, the numerical and experimental results are in good agreement with each other.

## V. CONCLUSION

The spatial distribution of entangled photons generated by non-linear crystal is of importance in the field of quantum information and quantum computation. We have observed a linear increase of thickness of the SPDC ring with beam radius of the pump beam.

We have also observed the formation of two concentric SPDC rings if the crystal is pumped with optical vortex beams. One of the reasons for generation of two rings is the dark core of optical vortex. The numerical and experimental widths of the SPDC ring are in good agreement with each other. The formation of two rings takes place when the pump beam size is more than the critical beam size. These observations would be useful

in the experiments to maximize the coincidence counts. Physically, the broadened SPDC is a consequence of the greater spread of pump transverse wave-vectors, resulting in phase matching for a greater spread of signal and idler transverse wave-vectors.

## ACKNOWLEDGMENTS

Authors wish to acknowledge Dr. A. K. Jha for fruitful discussion and experimental techniques. The numerical calculations reported in this article have been performed on a 3 TeraFlop high-performance cluster at Physical Research Laboratory (PRL), Ahmedabad, India.

- 
- [1] L. Zhang, A. B. U'ren, R. Erdmann, K. A. O'Donnell, C. Silberhorn, K. Banaszek, and I. A. Walmsley, *Generation of highly entangled photon pairs for continuous variable bell inequality violation*, Journal of Modern Optics **54**, 707–719 (2007).
  - [2] P. Kok, K. Nemoto, T. C. Ralph, J. P. Dowling, and G. J. Milburn, *Linear optical quantum computing with photonic qubits*, Reviews of Modern Physics **79**, 135–174 (2007).
  - [3] D. Burnham and D. Weinberg, *Observation of simultaneity in parametric production of optical photon pairs*, Physical Review Letters **25**, 84–87 (1970).
  - [4] C. Hong and L. Mandel, *Theory of parametric frequency down conversion of light*, Physical Review A **31**, 2409–2418 (1985).
  - [5] G. Molina-Terriza, J. P. Torres, and L. Torner, *Twisted photons*, Nature Physics **3**, 305–310 (2007).
  - [6] C. Law and J. Eberly, *Analysis and interpretation of high transverse entanglement in optical parametric down conversion*, Physical Review Letters **92**, 127903 (2004).
  - [7] A. Mair, A. Vaziri, G. Weihs, and A. Zeilinger, *Entanglement of the orbital angular momentum states of photons*, Nature **412**, 313316 (2001).
  - [8] J. C. Howell, R. S. Bennink, S. J. Bentley, and R. W. Boyd, *Realization of the einstein-podolsky-rosen paradox using momentum- and position-entangled photons from spontaneous parametric down conversion*, Physical Review Letters **92**, 210403 (2004).
  - [9] P. Kwiat, K. Mattle, H. Weinfurter, A. Zeilinger, A. Sergienko, and Y. Shih, *New high-intensity source of polarization-entangled photon pairs*, Physical Review Letters **75**, 4337–4341 (1995).
  - [10] C. Simon and J.-P. Poizat, *Creating single time-bin entangled photon pairs*, Physical Review Letters **94**, 030502 (2005).
  - [11] L. Allen, S. M. Barnett, and M. J. Padgett, *Optical angular momentum* (Institute of Physics Pub, 2003).
  - [12] M. Soskin, V. Gorshkov, M. Vasnetsov, J. Malos, and N. Heckenberg, *Topological charge and angular momentum of light beams carrying optical vortices*, Physical Review A **56**, 4064–4075 (1997).
  - [13] T. Kuga, Y. Torii, N. Shiokawa, T. Hirano, Y. Shimizu, and H. Sasada, *Novel optical trap of atoms with a doughnut beam*, Physical Review Letters **78**, 4713–4716 (1997).
  - [14] D. G. Grier, *A revolution in optical manipulation*, Nature **424**, 810–816 (2003).
  - [15] T. Brunet, J.-L. Thomas, and R. Marchiano, *Transverse shift of helical beams and subdiffraction imaging*, Physical Review Letters **105**, 034301 (2010).
  - [16] R. Ramírez-Alarcón, H. Cruz-Ramírez, and A. B. U'Ren, *Effects of crystal length on the angular spectrum of spontaneous parametric downconversion photon pairs*, Laser Physics **23**, 055204 (2013).
  - [17] T. Grayson and G. Barbosa, *Spatial properties of spontaneous parametric down-conversion and their effect on induced coherence without induced emission*, Physical Review A **49**, 2948–2961 (1994).
  - [18] R. Fickler, M. Krenn, R. Lapkiewicz, S. Ramelow, and A. Zeilinger, *Real-time imaging of quantum entanglement*, Scientific Reports **3**, 1914 (2013).
  - [19] R. W. Boyd, *Nonlinear optics* (Academic Press, 2003).
  - [20] O. Bryngdahl, *Formation of blazed gratings*, Journal of the Optical Society of America **60**, 140.1 (1970).